SCIENTIFIC JOURNAL - RECIMA21 ISSN 2675-6218

AGENT-BASED MODELING AND GRAPH-THEORETIC ANALYSIS OF ANGIOGENIC VASCULAR NETWORKS

MODELAGEM BASEADA EM AGENTES E ANÁLISE DE REDES VASCULARES ANGIOGÊNICAS POR MEIO DA TEORIA DOS GRAFOS

MODELADO BASADO EN AGENTES Y ANÁLISIS DE REDES VASCULARES ANGIOGÉNICAS MEDIANTE LA TEORÍA DE GRAFOS

Dandara Lorrayne do Nascimento[1], Ana Paula Alves[2], Leonardo Ferreira Calazans[3], Allbens P. F. Atman[4]

e7109158
https://doi.org/10.47820/recima21.v7i10.9158

PUBLISHED: 10/2026

ABSTRACT

Sprouting angiogenesis involves the interplay among endothelial signaling mechanisms, cell differentiation, and migration in response to angiogenic stimuli. This study aimed to quantitatively characterize the emergent properties of vascular networks generated by a mathematical and computational agent-based model integrating Notch–Delta–Jagged signaling and the cellular response to VEGF-A. Endothelial cells were individually represented on a two-dimensional lattice, and tip cell migration was governed by a stochastic rule weighted by local VEGF-A availability. Thirty independent simulations were performed, and the resulting vascular structures were skeletonized and converted into undirected graphs. The analysis included metrics related to nodal degree, branching, connectivity, shortest paths, and centrality. The results revealed an initial phase of rapid structural reorganization followed by relative stabilization of the main topological properties. The final networks exhibited a mean nodal degree of 2.46, with terminal nodes and simple branching nodes as the predominant structural classes. The largest connected component contained, on average, 87.6% of all nodes, indicating the formation of a dominant vascular structure. Betweenness centrality analysis revealed a heterogeneous distribution of the topological importance of nodes, while the main network metrics exhibited internal sampling stability across the analyzed simulations. Overall, the results indicate that the interaction between endothelial signaling and VEGF-A-weighted stochastic migration can generate vascular networks with consistent and organized topological properties, establishing a link between local cellular and molecular mechanisms and emergent vascular architecture.

KEYWORDS: *Angiogenesis. VEGF-A. Notch–Delta–Jagged. Agent-based modeling. Graph theory. Vascular networks.*

RESUMO

A angiogênese por brotamento envolve a interação entre mecanismos de sinalização endotelial, diferenciação celular e migração em resposta a estímulos. Este estudo teve como objetivo caracterizar quantitativamente as propriedades emergentes de redes vasculares geradas por um modelo matemático e computacional baseado em agentes, que integra a sinalização Notch–Delta–Jagged e a resposta celular ao VEGF-A. As células endoteliais foram representadas

[1] PhD candidate and MSc in Mathematical and Computational Modeling at the Federal Center for Technological Education of Minas Gerais (CEFET-MG). She is a faculty member in Mathematics at the Federal Institute of Education, Science and Technology of Southeast Minas Gerais (IF Sudeste MG), Bom Sucesso Campus, Brazil.
[2] BSc, MSc, and PhD in Physics from the Federal University of Minas Gerais (UFMG). She is a faculty member at the Federal University of Jequitinhonha and Mucuri Valleys (UFVJM), Brazil.
[3] BSc in Physics from the Federal University of Minas Gerais (UFMG), MSc in Mathematical and Computational Modeling from the Federal Center for Technological Education of Minas Gerais (CEFET-MG), and PhD in Physics from UFMG, Brazil.
[4] BSc and MSc in Physics from the Federal University of Minas Gerais (UFMG) and PhD in Sciences from UFMG. He completed postdoctoral research at Université Paris VI – Pierre et Marie Curie (2002–2004) and at UFMG (2004–2005). He is a professor at the Federal Center for Technological Education of Minas Gerais (CEFET-MG) and a member of the National Institute of Science and Technology – Complex Systems (INCT-SC), Brazil.

This article is published in open access under the Creative Commons Attribution 4.0 International (CC BY 4.0) license, which permits unrestricted use, distribution, and reproduction in any medium, provided that the original author and source are credited.

SCIENTIFIC JOURNAL - RECIMA21 ISSN 2675-6218

individualmente em uma malha bidimensional e a migração das células *tip* foi regida por uma regra estocástica ponderada pela disponibilidade local de VEGF-A. Foram realizadas 30 simulações independentes, e as estruturas vasculares resultantes foram esqueletizadas e convertidas em grafos não direcionados. A análise incluiu métricas relativas ao grau dos nós, à ramificação, à conectividade, aos caminhos mais curtos e à centralidade. Os resultados revelaram uma fase inicial de rápida reorganização estrutural, seguida de estabilização das principais propriedades topológicas. As redes finais apresentaram grau médio de 2,46, com predominância de nós terminais e nós de ramificação simples. O maior componente conectado continha, em média, 87,6% de todos os nós, indicando a formação de uma estrutura vascular dominante. A análise da centralidade de intermediação revelou uma distribuição heterogênea da importância topológica dos nós, enquanto as principais métricas da rede apresentaram estabilidade amostral interna entre as simulações analisadas. Em conjunto, os resultados indicam que a interação entre a sinalização endotelial e a migração estocástica ponderada pelo VEGF-A pode gerar redes vasculares com propriedades topológicas consistentes e organizadas, estabelecendo uma ligação entre mecanismos celulares e moleculares locais e a arquitetura vascular emergente.

PALAVRAS-CHAVE: Angiogênese. VEGF-A. Notch–Delta–Jagged. Modelagem Baseada em Agentes. Teoria dos Grafos. Redes Vasculares.

RESUMEN

La angiogénesis por brotación implica la interacción entre mecanismos de señalización endotelial, diferenciación celular y migración en respuesta a estímulos. Este estudio tuvo como objetivo caracterizar las propiedades emergentes de redes vasculares generadas por un modelo matemático y computacional basado en agentes que integra la señalización Notch–Delta–Jagged y la respuesta celular al VEGF-A. Las células endoteliales se representaron individualmente en una malla bidimensional, y la migración de las células tip se rigió por una regla ponderada por la disponibilidad local de VEGF-A. Se realizaron 30 simulaciones, y las estructuras vasculares resultantes se esqueletizaron y se convirtieron en grafos. El análisis incluyó métricas relacionadas con el grado de los nodos, la ramificación, la conectividad, los caminos más cortos y la centralidad. Los resultados revelaron una fase inicial de rápida reorganización estructural, seguida de una estabilización de las propiedades topológicas. Las redes finales presentaron un grado medio de 2,46, con predominio de nodos terminales y nodos de ramificación simple. El componente conectado más grande contenía, en promedio, el 87,6 % de todos los nodos, lo que indica la formación de una estructura vascular dominante. El análisis de la centralidad de intermediación reveló distribución heterogénea de la importancia topológica de los nodos, mientras que las principales métricas de la red mostraron estabilidad interna entre las simulaciones analizadas. Los resultados indican que la interacción entre la señalización endotelial y la migración estocástica ponderada por el VEGF-A puede generar redes vasculares con propiedades topológicas organizadas, estableciendo un vínculo entre los mecanismos celulares y la arquitectura vascular emergente.

PALABRAS CLAVE*: Angiogénesis. VEGF-A. Notch–Delta–Jagged. Modelado basado en agentes. Teoría de grafos. Redes vasculares.*

This article is published in open access under the Creative Commons Attribution 4.0 International (CC BY 4.0) license, which permits unrestricted use, distribution, and reproduction in any medium, provided that the original author and source are credited.

SCIENTIFIC JOURNAL - RECIMA21 ISSN 2675-6218

1. INTRODUCTION

Angiogenesis is the process by which new blood vessels form from pre-existing vasculature and plays a fundamental role in several physiological conditions, including embryonic development and tissue repair (Qi *et al.*, 2022; Geindreau *et al.*, 2022). Under conditions of hypoxia or increased nutrient demand, pro-angiogenic signals can promote endothelial cell activation and stimulate the formation of new vascular segments toward regions with greater oxygen and nutrient requirements (Boareto *et al.*, 2015a, 2015b).

Among the mechanisms involved in this process, the Notch and vascular endothelial growth factor (VEGF) signaling pathways are particularly important. Notch signaling participates in intercellular communication among endothelial cells and in the determination of their phenotypic states during vascular growth. Tip cells exhibit predominantly migratory behavior and guide newly forming vascular sprouts, whereas stalk cells contribute to the elongation and organization of the developing vascular segments. VEGF, in turn, is involved in endothelial cell activation and migratory responses to pro-angiogenic stimuli (Boareto *et al.*, 2015a, 2015b).

The interplay among molecular signaling, phenotypic differentiation, and cell migration spans multiple spatial and temporal scales, making mathematical and computational modeling an important tool for investigating angiogenesis. In this context, agent-based models allow endothelial cells and their local interactions with neighboring cells and the surrounding environment to be represented individually. These local interactions can give rise to collective patterns and spatial structures, thereby providing a framework for linking cellular mechanisms to the resulting vascular organization (Owen *et al.*, 2009; Bentley *et al.*, 2009; Scianna *et al.*, 2013).

Beyond the direct observation of the resulting structures, their representation as graphs enables a quantitative characterization of network organization. In this framework, nodes and edges represent structural elements and their connections, respectively, allowing properties related to network size, connectivity, branching, and topology to be analyzed. Metrics such as the numbers of nodes and edges, nodal degree, terminal nodes, branching nodes, centrality, and network distances provide complementary information about the structures generated by the model.

In this study, we consider a multicellular agent-based model constructed from the intracellular dynamics of the model adapted by Nascimento (2021), which is based on the formulation proposed by Boareto *et al.* (2015a). Endothelial cells explicitly occupy positions within the computational domain and interact locally with neighboring cells. Tip cell movement is governed by a stochastic rule in which the probability of migration to neighboring positions is weighted by the local extracellular availability of VEGF. The model therefore links intracellular

This article is published in open access under the Creative Commons Attribution 4.0 International (CC BY 4.0) license, which permits unrestricted use, distribution, and reproduction in any medium, provided that the original author and source are credited.

SCIENTIFIC JOURNAL - RECIMA21 ISSN 2675-6218

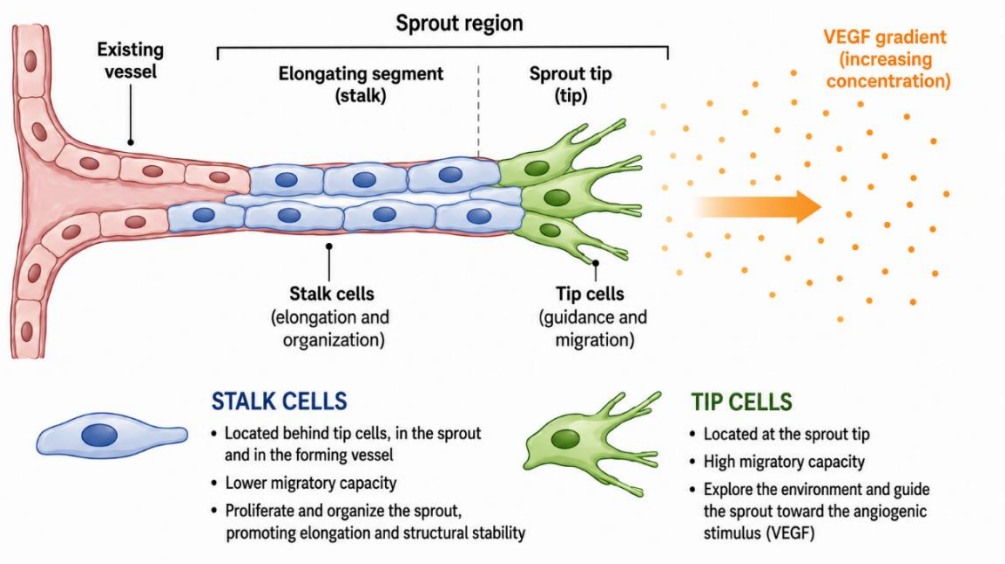
signaling, cellular state, local interactions, and spatial migration to the formation of vascular structures.

The aim of this study is to quantitatively characterize the emergent vascular networks generated by the agent-based model with VEGF-weighted migration. To this end, the simulated structures are represented as graphs and analyzed using metrics related to the numbers of nodes and edges, degree distribution, terminal and branching nodes, centrality, and network distances. The analysis of multiple independent realizations further enables the assessment of variability arising from the stochastic nature of the model and the consistency of the resulting topological properties.

2. ANGIOGENESIS AND ENDOTHELIAL SIGNALING

During sprouting angiogenesis, tip cells guide vascular growth toward angiogenic stimuli, whereas stalk cells support sprout elongation and organization (Boareto *et al.*, 2015a, 2015b; Bocci *et al.*, 2020; Rai *et al.*, 2022; Diez *et al.*, 2007; Ansari *et al.*, 2022). These phenotypes are illustrated in Figure 1.

Figure 1. Schematic representation of the endothelial cell phenotypes involved in angiogenic growth. Tip cells guide vascular sprouts toward VEGF-mediated angiogenic stimuli, whereas stalk cells remain associated with the developing vascular structure.



Tip–stalk differentiation is regulated in part by Notch signaling, activated when Notch receptors interact with Delta or Jagged ligands on adjacent cells and release NICD (Boareto *et al.*, 2015a, 2015b). Notch–Delta interactions promote lateral inhibition: cells with higher Delta

This article is published in open access under the Creative Commons Attribution 4.0 International (CC BY 4.0) license, which permits unrestricted use, distribution, and reproduction in any medium, provided that the original author and source are credited.

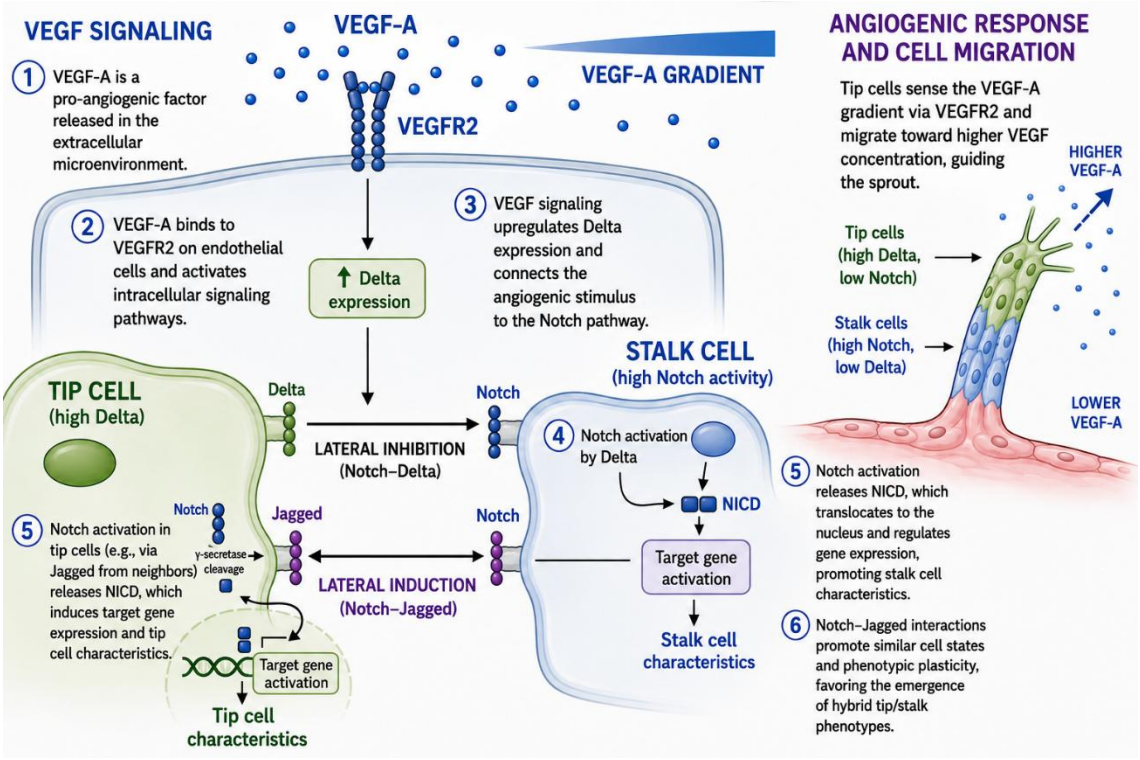
SCIENTIFIC JOURNAL - RECIMA21 ISSN 2675-6218

expression are associated with the tip state, while neighboring cells with greater Notch activity tend toward the stalk state (Beatus & Lendahl, 1998; Boareto *et al.*, 2015b; Bocci *et al.*, 2020). Notch–Jagged interactions can instead promote lateral induction and phenotypic plasticity (Boareto *et al.*, 2015a, 2015b; Bocci *et al.*, 2020).

Notch can interact with ligands expressed either by neighboring cells (*trans*) or by the same cell (*cis*), with these mechanisms contributing differently to signaling regulation (Boareto *et al.*, 2015a, 2015b). Both types of interaction are incorporated into the computational model.

VEGF-A binds endothelial receptors such as VEGFR2, influences Delta expression, and links the response to angiogenic stimuli with Notch-mediated phenotypic regulation (Boareto *et al.*, 2015a; Shibuya, 2011). Its extracellular distribution also guides tip-cell migration. Together, Notch–Delta–Jagged signaling and VEGF-A contribute to cellular differentiation and vascular growth, as summarized in Figure 2.

Figure 2. Schematic representation of the main interactions between the Notch–Delta–Jagged and VEGF signaling pathways considered in endothelial cell differentiation and behavior. Notch-mediated signaling participates in determining phenotypic states, whereas VEGF acts as an angiogenic stimulus and influences the migratory behavior of tip cells.



This article is published in open access under the Creative Commons Attribution 4.0 International (CC BY 4.0) license, which permits unrestricted use, distribution, and reproduction in any medium, provided that the original author and source are credited.

SCIENTIFIC JOURNAL - RECIMA21 ISSN 2675-6218

The following section describes how these signaling and migration mechanisms are represented in the multicellular model.

3. MATHEMATICAL AND COMPUTATIONAL MODEL

The mathematical and computational model used in this study describes endothelial cell dynamics through a spatially coupled multicellular approach based on interactions among the Notch–Delta–Jagged and VEGF signaling pathways. Each cell is individually represented on a two-dimensional lattice and is characterized by a set of intracellular variables that determine its molecular state and influence its phenotypic differentiation during vascular growth.

The computational domain is represented by a 140 × 140 square lattice, in which each position may correspond either to an endothelial cell or to an extracellular site available for occupation. Each agent is characterized by the intracellular concentrations of Notch (N), Delta (D), Jagged (J), NICD (I), intracellular VEGF (V), and VEGF receptor (VR). The temporal evolution of these variables is described by a coupled system of ordinary differential equations adapted from Boareto *et al.* (2015a) and the formulation employed by Nascimento (2021).

Interactions among agents are established through local signaling between neighboring cells. To represent these interactions, the model incorporates cis mechanisms, associated with proteins expressed within the same cell, and trans mechanisms, associated with signaling between adjacent cells. Spatial coupling is defined using a von Neumann neighborhood, allowing the concentrations of Notch, Delta, and Jagged in neighboring cells to influence the molecular dynamics of each agent.

In addition to intercellular signaling, the model explicitly accounts for the extracellular availability of VEGF. This factor is spatially distributed throughout the computational domain and contributes both to cellular molecular dynamics and to the direction of vascular growth. Thus, the model integrates three main components: intracellular protein dynamics, molecular coupling between neighboring cells, and the spatial influence of VEGF.

The governing equations of the model are given by Equation (1).

$$\frac{dN_i}{dt} = N_0 H^{s+}\left(I_i, \lambda_{I,N}\right) - N_i\left[\left(k_c D_i + k_t \langle D_j \rangle\right) + \left(k_c J_i + k_t \langle J_j \rangle\right)\right] - \gamma N_i \quad (1)$$

The Notch equation describes the temporal dynamics of the intracellular concentration of Notch receptors in cell i. The term $N_0 H^{s+}\left(I_i, \lambda_{I,N}\right)$ represents Notch production regulated by intracellular NICD levels through an activating Hill function. The central terms describe cis and trans interactions between Notch and the Delta and Jagged ligands. Cis interactions, proportional to k_c, occur between proteins located within the same cell, whereas trans interactions, associated

This article is published in open access under the Creative Commons Attribution 4.0 International (CC BY 4.0) license, which permits unrestricted use, distribution, and reproduction in any medium, provided that the original author and source are credited.

SCIENTIFIC JOURNAL - RECIMA21 ISSN 2675-6218

with k_t, represent lateral coupling between neighboring cells in the network. The final term corresponds to the natural degradation of the Notch protein at rate γ.

In the subsequent equations, the terms $\langle N_j \rangle, \langle D_j \rangle$ and $\langle J_j \rangle$ represent the spatial averages of the concentrations of Notch, Delta, and Jagged, respectively, within the von Neumann neighborhood. Furthermore, H^{s+} and H^{s-} denote Hill functions used to model gene activation and repression processes, respectively.

The dynamics of the Delta protein were modeled by considering its regulation by intracellular NICD and VEGF levels, in addition to lateral interactions mediated by Notch receptors located both in the same cell and in neighboring cells. The governing equation for Delta is given by Equation 2.

$$\frac{dD_i}{dt} = D_0 H^{s-}(I_i, \lambda_{I,D}) H^{s+}(V_i, \lambda_{V,D}) - k_c D_i N_i - k_t D_i \langle N_j \rangle - \gamma D_i \quad (2)$$

The Delta equation incorporates production mechanisms simultaneously regulated by Notch signaling and intracellular VEGF levels, establishing a coupling between cellular differentiation and angiogenic stimulation. The terms associated with cis and trans interactions describe the functional consumption of Delta during lateral coupling mediated by Notch receptors, whereas the final term represents the natural degradation of the protein.

Jagged was modeled as an important modulator of lateral signaling during the angiogenic process, directly influencing the mechanisms of phenotypic differentiation between tip and stalk cells. Its intracellular dynamics were described by Equation 3.

$$\frac{dJ_i}{dt} = J_0 H^{s+}(I_i, \lambda_{I,J}) - k_c J_i N_i - k_t J_i \langle N_j \rangle - \gamma J_i \quad (3)$$

The dynamics of Jagged include production regulated by intracellular NICD levels, in addition to cis and trans interactions mediated by Notch receptors. The terms proportional to k_c describe intracellular interactions between Jagged and Notch, whereas the terms associated with k_t represent lateral coupling between neighboring cells. The final term corresponds to the natural degradation of the protein.

The dynamics of NICD were modeled by considering the activation of Notch signaling mediated by trans interactions between Notch receptors and the Delta and Jagged ligands expressed by neighboring cells. The intracellular concentration of NICD was described by Equation 4.

$$\frac{dI_i}{dt} = N_i k_t [\langle D_j \rangle + \langle J_j \rangle] - \gamma_s I_i \quad (4)$$

NICD production depends directly on the lateral coupling between adjacent cells and is proportional to the trans interactions between Notch receptors and ligands present in the neighborhood of cell *i*. In this way, NICD acts as the main intracellular mediator of Notch signaling,

This article is published in open access under the Creative Commons Attribution 4.0 International (CC BY 4.0) license, which permits unrestricted use, distribution, and reproduction in any medium, provided that the original author and source are credited.

SCIENTIFIC JOURNAL - RECIMA21 ISSN 2675-6218

regulating the mechanisms responsible for phenotypic differentiation between tip and stalk cells. The final term of the equation represents the natural degradation of the protein.

The dynamics of the VEGF receptor were modeled by considering cellular response mechanisms to extracellular angiogenic stimulation. The intracellular concentration of VEGF receptors was described by Equation 5.

$$\frac{dV_{Ri}}{dt} = V_{R0}H^{s-}(I_i, \lambda_{I,V_R}) - k_t V_{Ri} V_{ext} - \gamma V_{Ri} \quad (5)$$

The production of VEGF receptors is regulated by intracellular NICD levels, establishing a coupling between Notch signaling and cellular sensitivity to the extracellular angiogenic gradient. The term associated with the interaction between V_{Ri} and V_{ext} represents receptor activation mediated by extracellular VEGF, whereas the final term describes the natural degradation of the protein. Consequently, the dynamics of VR contribute to the intracellular response to extracellular VEGF-A and to its coupling with Notch signaling.

The dynamics of intracellular VEGF were modeled by considering the uptake of extracellular angiogenic stimuli mediated by VEGF receptors expressed on the cell membrane. The intracellular VEGF concentration was described by Equation 6.

$$\frac{dV_i}{dt} = k_t V_{Ri} V_{ext} - \gamma_s V_i \quad (6)$$

The production of intracellular VEGF depends directly on the interaction between VEGF receptors and the extracellular angiogenic field V_{ext}, representing the internalization of the angiogenic stimulus by endothelial cells. The final term of the equation describes the natural degradation of intracellular VEGF.

Gene activation and repression mechanisms were modeled using shifted Hill functions of the form:

$$H^s(I_{i,j}, \lambda) = \frac{1}{1 + \left(\frac{I_{i,j}}{I_0}\right)^n} + \lambda \frac{\left(\frac{I_{i,j}}{I_0}\right)^n}{1 + \left(\frac{I_{i,j}}{I_0}\right)^n} \quad (7)$$

In Equation (7), the Hill coefficient controls the strength of NICD-mediated regulation, the threshold determines the concentration at which regulation changes, and the shift parameter specifies whether the function represents activation or repression.

Similarly, regulatory mechanisms mediated by intracellular VEGF were described using shifted Hill functions dependent on the concentration $V_{i,j}$ (Equation 8):

$$H^s(V_{i,j}, \lambda) = \frac{1}{1 + \left(\frac{V_{i,j}}{V_0}\right)^n} + \lambda \frac{\left(\frac{V_{i,j}}{V_0}\right)^n}{1 + \left(\frac{V_{i,j}}{V_0}\right)^n} \quad (8)$$

This article is published in open access under the Creative Commons Attribution 4.0 International (CC BY 4.0) license, which permits unrestricted use, distribution, and reproduction in any medium, provided that the original author and source are credited.

SCIENTIFIC JOURNAL - RECIMA21 ISSN 2675-6218

where V_0 represents the regulatory threshold associated with intracellular VEGF, while n corresponds to the Hill coefficient related to the strength of gene activation or repression mediated by the angiogenic stimulus.

As in the case of NICD-dependent functions, the parameter λ determines the type of regulation exerted by the shifted Hill function and may represent either activation (H^{s+}) or repression (H^{s-}) mechanisms.

Shifted Hill functions allow the representation of nonlinear regulatory mechanisms associated with intracellular signaling, reproducing NICD-mediated gene activation and repression processes.

The parameters used in the governing equations of the model were adapted from Boareto *et al.* (2015a) and are presented in Table 1.

Table 1. Parameters used in the simulations of the angiogenesis model, adapted from Boareto *et al.* (2015a)

Parameter	Value	Unit
N_0	1200	protein·h^{-1}
J_0	800	protein·h^{-1}
$D_0 = V_{R0}$	1000	protein·h^{-1}
$I_0 = V_0$	200	protein·h^{-1}
γ	0.1	h^{-1}
γ_s	0.5	h^{-1}
$\lambda_{I,N} = \lambda_{I,J} = \lambda_{V,D}$	2	Dimensionless
$\lambda_{I,D} = \lambda_{I,V_R}$	0	Dimensionless
$n_N = n_D = n_V = n_{V_R}$	2	Dimensionless
n_J	5	Dimensionless
k_t	2.5×10^{-5}	h^{-1}
k_c	5×10^{-4}	h^{-1}

Together, Equations (1–8) describe intracellular signaling and local coupling among endothelial agents. Their numerical solution provides the molecular states used in the spatial simulations. The implementation, migration rules, simulation conditions, and graph-based analyses are described in the following section.

This article is published in open access under the Creative Commons Attribution 4.0 International (CC BY 4.0) license, which permits unrestricted use, distribution, and reproduction in any medium, provided that the original author and source are credited.

SCIENTIFIC JOURNAL - RECIMA21 ISSN 2675-6218

4. MATERIALS AND METHODS

Simulations used the multicellular model described by Equations (1–6) on a 140 × 140 two-dimensional lattice, with each site either empty or occupied by an endothelial cell. The first row initially contained tip and stalk cells with probabilities of 33% and 67%, respectively; all other sites were empty. Agents interacted through a von Neumann neighborhood, with periodic boundary conditions along the columns. At each step, intracellular concentrations were updated using the governing equations and neighboring-cell concentrations.

Cell differentiation was updated throughout network evolution according to the molecular states of the agents. In the algorithm used for the simulations analyzed in this study, the formation of new tip cells at available positions was conditioned on intracellular Notch and Delta levels according to the criteria $N < 300$ and $D > 6000$. Vascular structure formation also occurred through tip cell migration because, following a successful displacement, the position previously occupied by the tip cell acquired the stalk phenotype. Thus, the spatial progression of the network resulted from the combination of cell differentiation, local molecular signaling, and tip cell movement.

Extracellular VEGF-A (Vext) was distributed as an increasing vertical gradient. Tip-cell migration was stochastic, with movement probabilities weighted by VEGF-A concentrations at the four neighboring sites. The probability of selecting a site was defined by Equation (9).

$$\boldsymbol{P_k = \frac{VEGF - A_{,k}}{\sum_{j=1}^{4} VEGF - A_{,j}}} \quad \textbf{(9)}$$

where $VEGF - A_{,k}$ represents the extracellular VEGF concentration at the position under consideration, and the summation corresponds to the concentrations at the four neighboring positions. Thus, positions with greater VEGF availability had a higher probability of being selected.

After a direction was selected, the occupancy status of the corresponding position was evaluated. When displacement occurred, the new position became occupied by a tip cell, whereas the previously occupied position acquired the stalk phenotype, resulting in the progressive elongation of the vascular structure. In addition, occupation of a position by a tip cell reduced the local extracellular VEGF concentration by half.

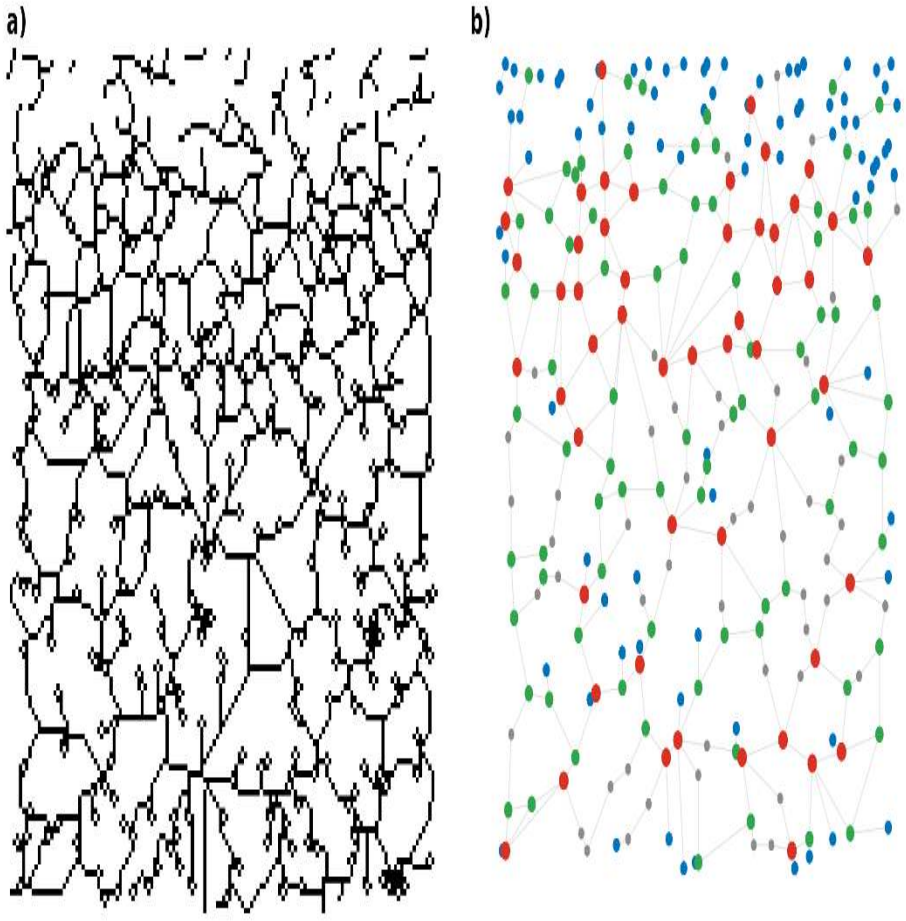
The model was implemented in C, and MATLAB was used for image processing and network analysis. Independent simulations used the same parameters; the number of realizations was assessed from the progressive stability of network metrics. At the end of each simulation, the vascular structure was converted to a binary image, skeletonized, and represented as an undirected graph. Nodes and edges represented structural elements and their connections, while node positions preserved the skeleton's spatial organization.

This article is published in open access under the Creative Commons Attribution 4.0 International (CC BY 4.0) license, which permits unrestricted use, distribution, and reproduction in any medium, provided that the original author and source are credited.

SCIENTIFIC JOURNAL - RECIMA21 ISSN 2675-6218

For the topological analysis, nodes were classified according to their nodal degree k, defined as the number of edges incident to each node. Nodes with $k = 1$ were classified as terminal nodes, those with $k = 2$ as intermediate nodes, nodes with $k = 3$ as simple branching nodes, and those with $k \geq 4$ as higher-order junctions. More generally, nodes with $k \geq 3$ were classified as branching nodes. Figure 3 shows the skeletonized network and its corresponding graph representation for representative simulation 4 at the final recorded state.

Figure 3. Representation of the vascular network for topological analysis. (a) Skeletonized vascular network corresponding to recorded state 196 of representative simulation 4. (b) Undirected graph obtained from the skeletonized network while preserving its spatial organization. Nodes are classified according to nodal degree k: terminal nodes ($k = 1$, blue), intermediate nodes ($k = 2$, gray), simple branching nodes ($k = 3$, green), and higher-order junctions ($k \geq 4$, red). Edges represent the connections between network nodes.



For visualization purposes, one representative realization was selected from the 30 simulations. For each simulation, a standardized distance from the ensemble mean was

This article is published in open access under the Creative Commons Attribution 4.0 International (CC BY 4.0) license, which permits unrestricted use, distribution, and reproduction in any medium, provided that the original author and source are credited.

SCIENTIFIC JOURNAL - RECIMA21 ISSN 2675-6218

calculated using the mean degree, number of branching nodes, fraction of nodes in the largest connected component, and mean shortest-path length.

Topological characterization was performed individually for each network. The number of nodes and edges, mean degree, maximum degree, and degree distribution were determined, together with the number and proportion of terminal nodes, intermediate nodes, simple branching nodes, and higher-order junctions. The number of connected components and the number and fraction of nodes belonging to the largest connected component were also determined.

Path-related and centrality properties were evaluated within the largest connected component of each network to prevent disconnected components from affecting the interpretation of topological distances. Betweenness, closeness, and eigenvector centralities were calculated. For betweenness and closeness centralities, the spatial lengths of the edges were used as traversal costs. Eigenvector centrality was calculated from the adjacency structure of the network without weighting by edge length. Based on shortest-path distances weighted by edge length, the mean shortest-path length and diameter of the largest connected component were determined. In addition, the mean distance between directly connected branching nodes was calculated.

Each independent simulation was treated as a unit of analysis. Thus, statistics describing network properties were calculated across the 30 independent realizations rather than by treating individual nodes as statistical replicates. For each metric, measures of central tendency and dispersion were calculated, together with 95% confidence intervals, thereby preserving the variability among independent realizations. The confidence intervals were estimated using the bias-corrected and accelerated (BCa) bootstrap method with 5,000 resamples. In addition, estimates obtained from cumulative sets of 10, 20, and 30 simulations were compared to assess the internal sampling stability of the main topological properties.

5. RESULTS

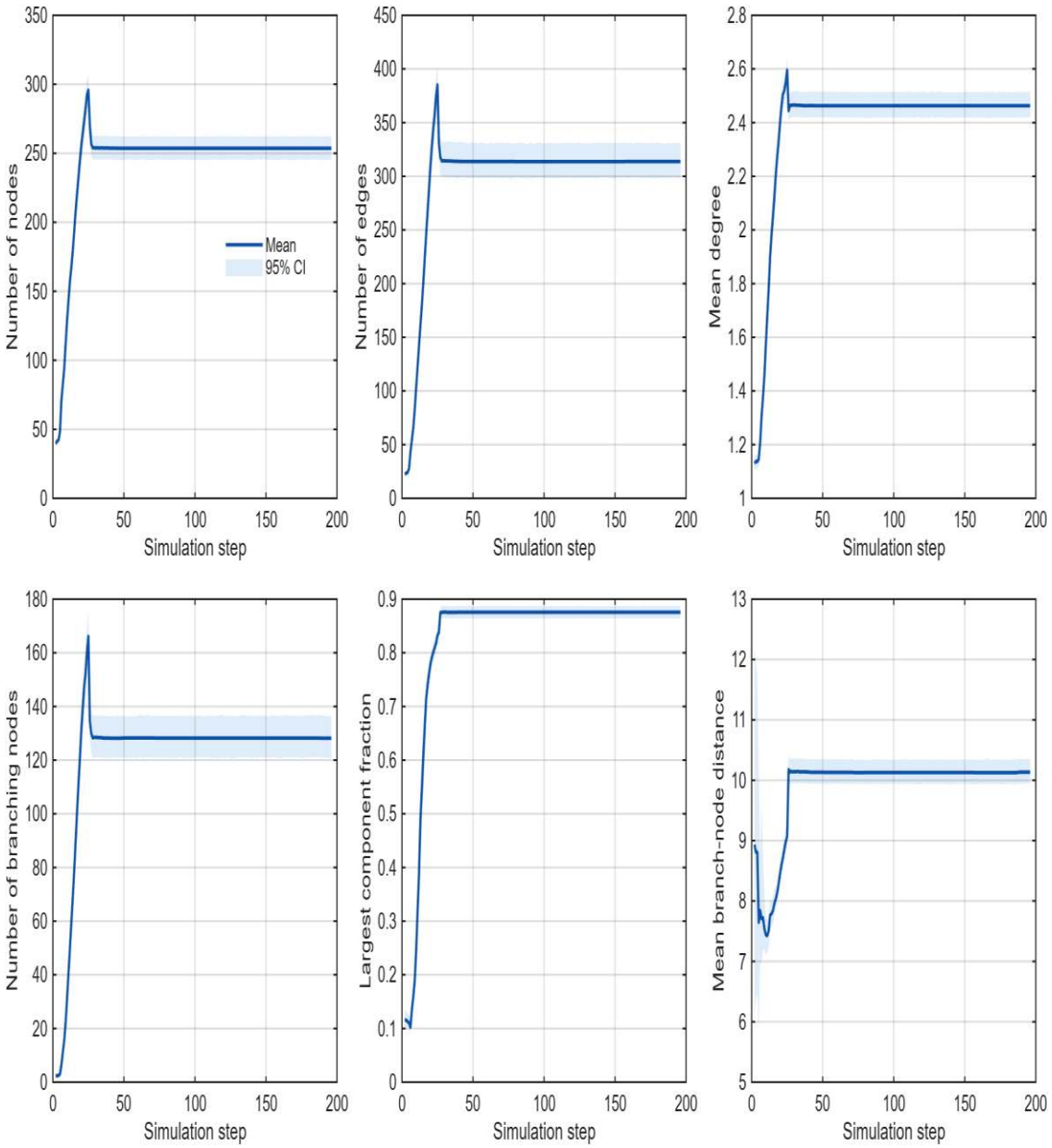
5.1. Temporal Evolution of Network Organization

The temporal evolution of the vascular networks revealed an initial phase of rapid structural reorganization, followed by the establishment of a comparatively stable topological regime. Figure 4 shows the evolution, over 19,600 simulation steps, of six global network properties: number of nodes, number of edges, mean degree, number of branching nodes, fraction of nodes belonging to the largest connected component, and mean distance between directly connected branching nodes. The curves represent the mean values obtained across the 30 independent simulations, whereas the shaded regions represent the corresponding 95% confidence intervals.

This article is published in open access under the Creative Commons Attribution 4.0 International (CC BY 4.0) license, which permits unrestricted use, distribution, and reproduction in any medium, provided that the original author and source are credited.

SCIENTIFIC JOURNAL - RECIMA21 ISSN 2675-6218

Figure 4. Temporal evolution of the main topological properties of the simulated vascular networks. Mean trajectories obtained from 30 independent simulations are shown for the number of nodes, number of edges, mean degree, number of branching nodes, fraction of nodes belonging to the largest connected component, and mean distance between directly connected branching nodes. Shaded regions represent 95% bootstrap confidence intervals. Time is expressed in discrete simulation steps.



During the initial phase, the numbers of nodes and edges increased rapidly, indicating substantial formation and reorganization of vascular structures. A similar pattern was observed

This article is published in open access under the Creative Commons Attribution 4.0 International (CC BY 4.0) license, which permits unrestricted use, distribution, and reproduction in any medium, provided that the original author and source are credited.

SCIENTIFIC JOURNAL - RECIMA21 ISSN 2675-6218

for the mean degree and number of branching nodes, which increased rapidly during the early stages, reached transient maxima, and subsequently decreased toward relatively stable values. After approximately 3,000–4,000 simulation steps, the main structural properties exhibited only minor fluctuations around approximately constant mean values. At the end of the simulations, the networks contained an average of 253.63 nodes (95% CI: 245.33–262.17) and 313.73 edges (95% CI: 298.83–331.43), with a mean degree of 2.463 (95% CI: 2.420–2.517). The mean number of branching nodes was 128.20 (95% CI: 120.79–136.17).

Global network connectivity was also established predominantly during the initial phase. The fraction of nodes belonging to the largest connected component increased rapidly and subsequently remained near a constant value. At the end of the simulations, this component contained, on average, 87.55% of the nodes (95% CI: 86.38–88.68%). Despite the persistence of disconnected components, this result shows that most network elements were integrated into a dominant vascular structure.

At the end of the simulations, the mean distance between directly connected branching nodes was 10.14 spatial units (95% CI: 9.94–10.35), indicating the maintenance of a characteristic spacing between branching regions after the initial reorganization phase.

These trajectories indicate an early phase of rapid topological reorganization followed by relative stabilization; this does not imply that cellular or molecular dynamics have ceased.

5.2. Topological Organization of the Final Vascular Networks

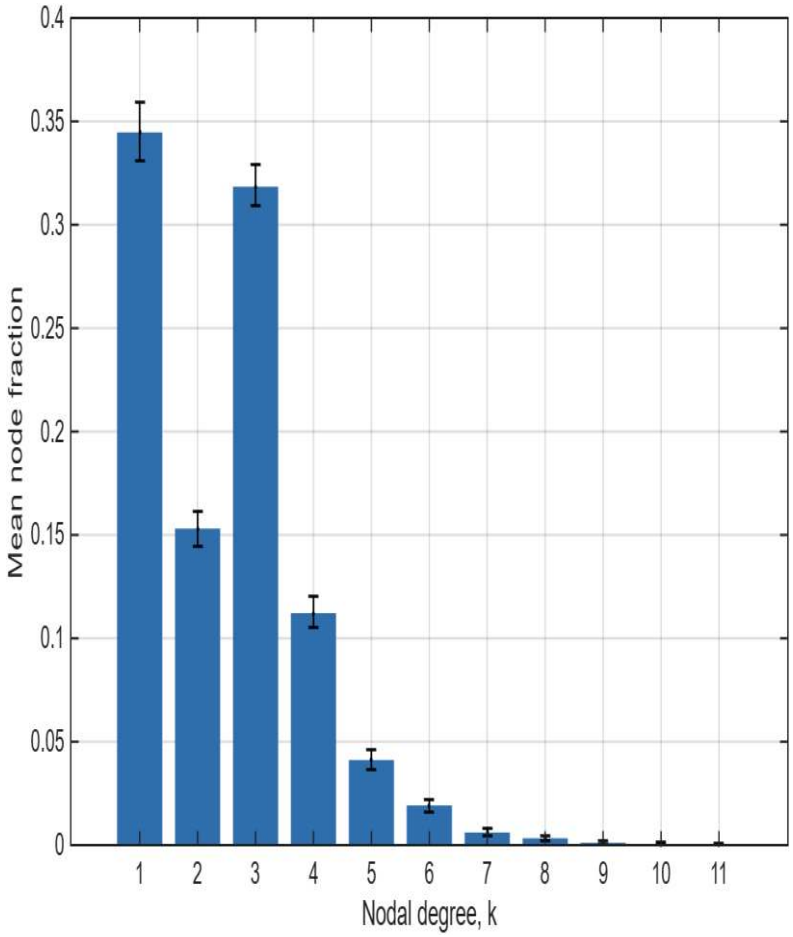
Analysis of the networks at the final recorded state showed that the resulting vascular organization was characterized by a combination of terminal nodes, intermediate nodes, and different branching orders. Across the 30 independent simulations, the networks exhibited a mean degree of 2.463 (95% CI: 2.420–2.517), whereas the mean maximum degree was 8.43 (95% CI: 8.03–8.87). However, higher-degree nodes became progressively less frequent, indicating that the largest degree values corresponded to localized features of the network architecture rather than its predominant organization.

The degree distribution further illustrates this pattern (Figure 5). Terminal nodes, with degree $k = 1$, were the most frequent category, accounting for an average of 34.46% of all nodes (95% CI: 33.09–35.91%). Nodes with $k = 3$, corresponding to simple branching nodes, constituted the second most prevalent category, accounting for 31.84% (95% CI: 30.90–32.89%). Intermediate nodes ($k = 2$) represented 15.31% of the network (95% CI: 14.42–16.17%).

This article is published in open access under the Creative Commons Attribution 4.0 International (CC BY 4.0) license, which permits unrestricted use, distribution, and reproduction in any medium, provided that the original author and source are credited.

SCIENTIFIC JOURNAL - RECIMA21 ISSN 2675-6218

Figure 5. Nodal degree distribution in the simulated vascular networks. Bars represent the mean proportion of nodes with each degree k, calculated across the 30 independent simulations. Error bars represent 95% confidence intervals obtained using the BCa bootstrap method with 5,000 resamples.



Although nodes with degree $k \geq 4$ were identified across the networks, their frequency decreased markedly as degree increased. Nodes with $k = 4$ represented, on average, 11.22% of the network, whereas nodes with $k = 5$ and $k = 6$ accounted for approximately 4.12% and 1.92%, respectively. For $k \geq 7$, each individual degree class represented less than 1% of all nodes. The highest degree observed across the simulations was $k = 11$, although its mean frequency was below 0.1%.

When considered together, simple branching nodes ($k = 3$) and higher-order junctions ($k \geq 4$) accounted for an average of 50.23% of all nodes (95% CI: 48.73–51.85%). Higher-order junctions alone represented 18.39% (95% CI: 17.42–19.76%). Thus, although a substantial

This article is published in open access under the Creative Commons Attribution 4.0 International (CC BY 4.0) license, which permits unrestricted use, distribution, and reproduction in any medium, provided that the original author and source are credited.

SCIENTIFIC JOURNAL - RECIMA21 ISSN 2675-6218

proportion of the network consisted of elements involved in branching, the architecture was dominated by lower-order branching, with a progressive decrease in the occurrence of higher-degree junctions.

5.3. Global Connectivity and Path Organization

The final networks consisted of multiple connected components, with an average of 13.97 components per simulation (95% CI: 12.87–15.00). Despite this fragmentation, the largest connected component contained most of the vascular structure, with an average of 222.30 nodes (95% CI: 213.37–230.69), corresponding to 87.55% of the total number of nodes in each network (95% CI: 86.38–88.68%).

Shortest-path analysis within the largest connected component yielded a mean shortest-path length of 93.36 spatial units (95% CI: 92.71–94.05). The mean network diameter was 224.19 spatial units (95% CI: 220.88–228.39), representing the longest shortest-path distance between two nodes within the dominant component. These results show that most of the vascular structure was integrated into an extensive main component, although smaller components remained spatially disconnected.

The mean distance between directly connected branching nodes was 10.14 spatial units (95% CI: 9.94–10.35). Together with the temporal stabilization observed for this metric, this result indicates that the final simulation regime exhibited relatively consistent spacing between directly connected branching regions.

5.4. Centrality and Structural Heterogeneity of the Network

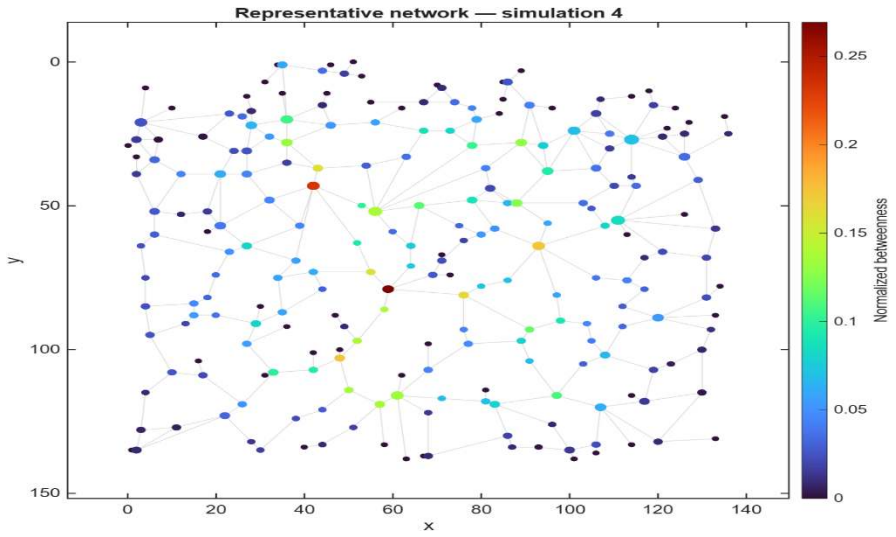
Centrality analysis was performed on the largest connected component of each simulation to characterize the relative importance of nodes in the organization of network paths. Normalized betweenness centrality had a mean value of 0.0417 (95% CI: 0.0403–0.0431), whereas the median was 0.0267 (95% CI: 0.0255–0.0278). The maximum betweenness value within each network was substantially higher, with a mean of 0.2338 (95% CI: 0.2213–0.2464).

The difference between mean and maximum betweenness values indicates a heterogeneous distribution of node participation in the shortest paths of the network. Whereas most nodes exhibited low betweenness centrality, a relatively small subset displayed considerably higher values, occupying positions traversed by a substantial proportion of the shortest paths within the main component. This heterogeneity can be observed spatially in the representative network shown in Figure 6.

This article is published in open access under the Creative Commons Attribution 4.0 International (CC BY 4.0) license, which permits unrestricted use, distribution, and reproduction in any medium, provided that the original author and source are credited.

SCIENTIFIC JOURNAL - RECIMA21 ISSN 2675-6218

Figure 6. Spatial distribution of betweenness centrality in the representative network. Largest connected component of representative simulation 4 at recorded state 196. Node color represents normalized betweenness centrality, with increasing values indicated by the color scale. Node size varies according to nodal degree. Edges represent network connections.



In the representative network, high betweenness values were concentrated in nodes connecting different regions of the main component, while many peripheral nodes had values close to zero. Across simulations, maximum betweenness ranged from 0.175 to 0.303.

For the other centrality measures, mean closeness centrality was 5.03×10^{-5} (95% CI: 4.83×10^{-5}–5.27×10^{-5}), whereas mean eigenvector centrality was 0.00455 (95% CI: 0.00438–0.00476). These measures complement the structural characterization of the largest connected component, whereas the spatial distribution of betweenness centrality more directly highlights the presence of regions with different levels of participation in network path organization.

6. DISCUSSION

The results show that the combination of local endothelial signaling and migration weighted by VEGF-A availability can generate vascular networks with emergent topological organization. The temporal evolution revealed an initial phase of rapid reorganization followed by relative stabilization of the main network properties. This behavior is consistent with the dynamics of sprouting angiogenesis, in which tip cells guide sprout advancement and stalk cells contribute to their extension and organization (Gerhardt *et al.*, 2003; Blanco & Gerhardt, 2013).

The spatial availability of VEGF-A plays an important role in this process. Tip cells respond to the extracellular distribution of VEGF-A, whose gradients contribute to filopodial

This article is published in open access under the Creative Commons Attribution 4.0 International (CC BY 4.0) license, which permits unrestricted use, distribution, and reproduction in any medium, provided that the original author and source are credited.

SCIENTIFIC JOURNAL - RECIMA21 ISSN 2675-6218

orientation and migration during sprouting (Gerhardt *et al.*, 2003). In the model, this mechanism is represented by a probabilistic rule that weights the direction of movement according to local VEGF-A availability, thereby combining spatial guidance with stochastic variability. The interaction among signaling, tip-cell selection, and migration has also been identified as an important determinant of emergent angiogenic organization in computational models (Bentley *et al.*, 2009).

The response to VEGF-A is associated with Notch–Delta signaling, which contributes to the functional differentiation between tip and stalk states (Hellström *et al.*, 2007; Blanco & Gerhardt, 2013). Alterations in Dll4–Notch signaling can increase tip-cell formation and vascular branching (Hellström *et al.*, 2007; Suchting *et al.*, 2007), whereas VEGF-induced Dll4 contributes to restricting excessive sprouting (Lobov *et al.*, 2007). Jagged also participates in this regulation and can antagonize Dll4–Notch-mediated signaling (Benedito *et al.*, 2009). Theoretical models further indicate that Notch–Delta–Jagged interactions can modify tip–stalk fate decisions and angiogenic patterns (Boareto *et al.*, 2015a, 2015b). These findings provide biological support for the mechanisms incorporated into the model, although they do not allow specific topological properties to be attributed to individual molecular components.

The final networks were characterized primarily by terminal nodes and low-order branching, whereas higher-degree junctions became progressively less frequent. In addition, the largest connected component contained approximately 87.6% of all nodes, indicating the formation of a dominant vascular structure. Representing the skeletonized structures as graphs extends their characterization beyond morphological descriptors by enabling the analysis of properties related to degree, connectivity, and paths, an approach also used in the quantitative analysis of endothelial networks (Okoro *et al.*, 2025). The formation of a dominant component is also consistent with the progressive establishment of connections between sprouts during angiogenesis (Blanco & Gerhardt, 2013).

Path-based and centrality measures complemented this characterization. The stabilization of distances between branching nodes indicates the emergence of relatively consistent spatial organization, whereas betweenness centrality revealed that certain nodes occupy positions of greater importance in the organization of shortest paths. These metrics distinguish local connectivity from global structural importance, consistent with applications of graph theory to angiogenic networks (Okoro *et al.*, 2025). However, they should be interpreted exclusively as topological properties because the model does not incorporate hemodynamic variables.

The model has limitations arising from its two-dimensional representation and the absence of components such as the extracellular matrix, lumen formation, mural cells, blood flow, and hemodynamic properties. Computational simulation steps were also not directly calibrated to

This article is published in open access under the Creative Commons Attribution 4.0 International (CC BY 4.0) license, which permits unrestricted use, distribution, and reproduction in any medium, provided that the original author and source are credited.

SCIENTIFIC JOURNAL - RECIMA21 ISSN 2675-6218

a biological time scale, and the individual effects of molecular mechanisms on network topology were not isolated. Although VEGF, Dll4–Notch, and Jagged are associated with the regulation of tip and stalk behaviors and vascular sprouting (Hellström *et al.*, 2007; Benedito *et al.*, 2009; Blanco & Gerhardt, 2013), specific perturbation analyses would be required to quantify their individual contributions.

Overall, the results support a multiscale interpretation of simulated vascular formation. Notch–Delta–Jagged signaling contributes to the determination of endothelial cell states, whereas local VEGF-A availability probabilistically guides migration. Repeated local interactions generate emergent properties related to branching, connectivity, paths, and centrality. Thus, the combination of agent-based modeling and graph theory provides a quantitative approach for relating molecular and cellular mechanisms to the topological organization of vascular networks, consistent with recent applications of graph analysis to angiogenic networks (Okoro *et al.*, 2025).

7. CONCLUSIONS

The agent-based model linked Notch–Delta–Jagged signaling, endothelial phenotypic states, and VEGF-A-weighted stochastic migration to the formation of vascular networks. Across 30 independent simulations, the networks underwent rapid initial reorganization followed by relative topological stabilization. Their final structure was dominated by terminal and low-order branching nodes, with a mean degree near 2.46; approximately 87.6% of nodes belonged to the largest connected component.

Graph-based analysis extended the characterization of these networks beyond their visual morphology. Branching distances indicated relatively consistent spatial organization, whereas betweenness centrality revealed heterogeneous participation of nodes in shortest paths. The study's main contribution is therefore the quantitative connection between local cellular mechanisms and emergent network topology.

The model remains a simplified representation of sprouting angiogenesis because it is two-dimensional, does not include blood flow or hemodynamic properties, and does not calibrate simulation steps to biological time. Future perturbation analyses may clarify the individual effects of the incorporated molecular mechanisms on network topology and extend the model toward vascular function.

This study was financed in part by the Coordenação de Aperfeiçoamento de Pessoal de Nível Superior – Brasil (CAPES).

REFERENCES

Ansari, M. J., *et al.* (2022). Cancer combination therapies by angiogenesis inhibitors: A comprehensive review. *Cell Communication and Signaling, 20*(1), 1–23.

This article is published in open access under the Creative Commons Attribution 4.0 International (CC BY 4.0) license, which permits unrestricted use, distribution, and reproduction in any medium, provided that the original author and source are credited.

SCIENTIFIC JOURNAL - RECIMA21 ISSN 2675-6218

Beatus, P., & Lendahl, U. (1998). Notch and neurogenesis. *Journal of Neuroscience Research, 54*(2), 125–136.

Benedito, R., Roca, C., Sörensen, I., Adams, S., Gossler, A., Fruttiger, M., & Adams, R. H. (2009). The Notch ligands Dll4 and Jagged1 have opposing effects on angiogenesis. *Cell, 137*(6), 1124–1135. https://doi.org/10.1016/j.cell.2009.03.025

Bentley, K., *et al.* (2009). Tipping the balance: Robustness of tip cell selection, migration and fusion in angiogenesis. *PLoS Computational Biology, 5*(10), e1000549.

Blanco, R., & Gerhardt, H. (2013). VEGF and Notch in tip and stalk cell selection. *Cold Spring Harbor Perspectives in Medicine, 3*(1), a006569. https://doi.org/10.1101/cshperspect.a006569

Boareto, M., Jolly, M. K., Ben-Jacob, E., & Onuchic, J. N. (2015a). Jagged mediates differences in normal and tumor angiogenesis by affecting tip-stalk fate decision. *Proceedings of the National Academy of Sciences of the United States of America, 112*(29), E3836–E3844. https://doi.org/10.1073/pnas.1511814112

Boareto, M., Jolly, M. K., Lu, M., Onuchic, J. N., Clementi, C., & Ben-Jacob, E. (2015b). Jagged–Delta asymmetry in Notch signaling can give rise to a sender/receiver hybrid phenotype. *Proceedings of the National Academy of Sciences of the United States of America, 112*(5), E402–E409. https://doi.org/10.1073/pnas.1416287112

Bocci, F., Onuchic, J. N., & Jolly, M. K. (2020). Understanding the principles of pattern formation driven by Notch signaling by integrating experiments and theoretical models. *Frontiers in Physiology, 11*, 929.

Diez, H., *et al.* (2007). Hypoxia-mediated activation of Dll4-Notch-Hey2 signaling in endothelial progenitor cells and adoption of arterial cell fate. *Experimental Cell Research, 313*(1), 1–9.

Geindreau, M., Bruchard, M., & Vegran, F. (2022). Role of cytokines and chemokines in angiogenesis in a tumor context. *Cancers, 14*(10), 2446.

Gerhardt, H., Golding, M., Fruttiger, M., Ruhrberg, C., Lundkvist, A., Abramsson, A., Jeltsch, M., Mitchell, C., Alitalo, K., Shima, D., & Betsholtz, C. (2003). VEGF guides angiogenic sprouting utilizing endothelial tip cell filopodia. *Journal of Cell Biology, 161*(6), 1163–1177. https://doi.org/10.1083/jcb.200302047

Hellström, M., Phng, L. K., Hofmann, J. J., *et al.* (2007). Dll4 signalling through Notch1 regulates formation of tip cells during angiogenesis. *Nature, 445*, 776–780. https://doi.org/10.1038/nature05571

Lobov, I. B., Renard, R. A., Papadopoulos, N., Gale, N. W., Thurston, G., Yancopoulos, G. D., & Wiegand, S. J. (2007). Delta-like ligand 4 (Dll4) is induced by VEGF as a negative regulator of angiogenic sprouting. *Proceedings of the National Academy of Sciences of the United States of America, 104*(9), 3219–3224. https://doi.org/10.1073/pnas.0611206104

Nascimento, D. L. (2021). *Modelo matemático para a angiogênese baseado na dinâmica das vias de sinalização Notch e VEGF* [Master's thesis, Centro Federal de Educação Tecnológica de Minas Gerais].

Okoro, G., Wityk, P., Nelappana, M. B., *et al.* (2025). A graph-theoretic framework for quantitative analysis of angiogenic networks. *BioData Mining, 18*, Article 69. https://doi.org/10.1186/s13040-025-00478-1

This article is published in open access under the Creative Commons Attribution 4.0 International (CC BY 4.0) license, which permits unrestricted use, distribution, and reproduction in any medium, provided that the original author and source are credited.

SCIENTIFIC JOURNAL - RECIMA21 ISSN 2675-6218

Owen, M. R., *et al.* (2009). Angiogenesis and vascular remodelling in normal and cancerous tissues. *Journal of Mathematical Biology, 58*(4–5), 689–721.

Qi, S., *et al.* (2022). Novel drugs with high efficacy against tumor angiogenesis. *International Journal of Molecular Sciences, 23*(13), 6934.

Rai, V., Moellmer, R., & Agrawal, D. K. (2022). Stem cells and angiogenesis: Implications and limitations in enhancing chronic diabetic foot ulcer healing. *Cells, 11*(15), 2287.

Scianna, M., Bell, C. G., & Preziosi, L. (2013). A review of mathematical models for the formation of vascular networks. *Journal of Theoretical Biology, 333*, 174–209.

Shibuya, M. (2011). Vascular endothelial growth factor (VEGF) and its receptor (VEGFR) signaling in angiogenesis: A crucial target for anti- and pro-angiogenic therapies. *Genes & Cancer, 2*(12), 1097–1105.

Suchting, S., Freitas, C., Le Noble, F., Benedito, R., Bréant, C., Duarte, A., & Eichmann, A. (2007). The Notch ligand Delta-like 4 negatively regulates endothelial tip cell formation and vessel branching. *Proceedings of the National Academy of Sciences of the United States of America, 104*(9), 3225–3230. https://doi.org/10.1073/pnas.0611177104

This article is published in open access under the Creative Commons Attribution 4.0 International (CC BY 4.0) license, which permits unrestricted use, distribution, and reproduction in any medium, provided that the original author and source are credited.